(2) D. G. Pillsbury and D. H. Busch, *J. Am. Chem. Soc.*, **98**, 7836 (1976).
(3) K. Kubokura, H. Okawa, and S. Kida, *Bull. Chem. Soc. Jpn.*, **51** (7), 2036 (1978).
(4) G. McLendon and A. E. Martell, *Coord. Chem. Rev.*, **19**, 1 (1976).
(5) D. P. Riley, J. A. Stone, and D. H. Busch, *J. Am. Chem. Soc.*, **98**, 1752 (1976).
(6) D. P. Riley, Ph.D. Thesis, The Ohio State University, 1975.
(7) B. J. Hathaway, D. E. Billing, P. Nicholls, and I. M. Proctor, *J. Chem. Soc. A*, 319 (1969).
(8) B. J. Hathaway, I. M. Proctor, R. C. Slade, and A. A. G. Tomlinson, *J. Chem. Soc. A*, 2219 (1969).
(9) M. Honda and G. Schwarzenbach, *Helv. Chim. Acta*, **40**, 27 (1957).
(10) B. R. James, M. Parris, and R. J. P. Williams, *J. Chem. Soc.*, 4630 (1961).
(11) B. J. Hathaway and A. A. G. Tomlinson, *Coord. Chem. Rev.*, **5**, 1 (1970).
(12) A. A. G. Tomlinson, B. J. Hathaway, D. E. Billing, and P. Nicholls, *J. Chem. Soc. A*, 65 (1969).
(13) B. J. Hathaway and D. E. Billing, *Coord. Chem. Rev.*, **5**, 143 (1970).
(14) R. J. Dudley, R. J. Fereday, B. J. Hathaway, and P. G. Hodgson, *J. Chem. Soc., Dalton Trans.*, 1341 (1972).
(15) C. M. Cuzy, J. B. Raynor, and M. C. R. Symons, *J. Chem. Soc. A*, 2299 (1969).
(16) L. Y. Martin, S. C. Jackels, A. M. Tait, and D. H. Busch, *J. Am. Chem. Soc.*, **99**, 4029 (1977).
(17) A. H. Maki and B. R. McGarvey, *J. Chem. Phys.*, **29**, 31 (1958).
(18) D. Kivelson and R. Neiman, *J. Chem. Phys.*, **35**, 149 (1961).
(19) J. W. Dodd and N. S. Hush, *J. Chem. Soc.*, 4607 (1964).
(20) D. W. Clark and N. S. Hush, *J. Am. Chem. Soc.*, **87**, 4238 (1965).
(21) M. Zerner and M. Gouterman, *Theor. Chim. Acta*, **4**, 44 (1966).
(22) F. V. Lovecchio, E. S. Gore, and D. H. Busch, *J. Am. Chem. Soc.*, **96**, 3109 (1974).
(23) V. Katovic, L. Lindoy, and D. H. Busch, *J. Chem. Educ.*, **49**, 117 (1972).
(24) A. K. Wiersema and J. J. Windle, *J. Phys. Chem.*, **68**, 983 (1964).
(25) G. M. Larin, G. V. Panova, and E. G. Rukhadze, *J. Struct. Chem. (Engl. Transl.)*, **6**, 664 (1965).

Contribution from the Department of Chemistry,
University of Calgary, Calgary, Alberta, Canada, T2N 1N4

A Theoretical Study of the Ethylene–Metal Bond in Complexes between Cu^+, Ag^+, Au^+, Pt^0, or Pt^{2+} and Ethylene, Based on the Hartree–Fock–Slater Transition-State Method

TOM ZIEGLER and ARVI RAUK*

Received December 4, 1978

An analysis based on the Hartree–Fock–Slater transition-state method is given of the metal–ethylene bond in the ion–ethylene complexes Cu^+–C_2H_4, Ag^+–C_2H_4, and Au^+–C_2H_4 as well as in complexes with $PtCl_3^-$ and $Pt(PH_3)_2$. The contribution from σ donation to the bonding energy was found to be equally important for all three complexes with the ions, whereas the contribution from the π back-donation was found to be important only for the Cu complex. A similar analysis of $Pt(Cl)_3^-$–C_2H_4 and $Pt(PH_3)_2$–C_2H_4 showed that the position of ethylene perpendicular to the coordination plane of $Pt(Cl)_3^-$ in Zeise's salt is caused by steric factors, whereas the position of ethylene in $Pt(PH_3)_2$–C_2H_4 is due to electronic factors, specificially π back-donations.

1. Introduction

The bonding in transition-metal complexes has come under close scrutiny in recent years by the powerful combination of semiempirical calculations and use of simple perturbation theory (PMO) as employed by Hoffmann and his co-workers, as well as others.[1] Such systems, because of their size, are not readily amenable to study by ab initio methods, although a number of attempts have been made when advantage could be taken of high symmetry. Hartree–Fock calculations are very time consuming and artifacts introduced as a consequence of unavoidable limitations of the basis set and neglect of electron correlation are not readily identified and ruled out. Although the faster Hartree–Fock–Slater (HFS) method, using the transition-state approximation,[2] has been used numerous times[3-5] with considerable success for the calculation of ionization potentials and electronic excitation energies, little insight has yet been achieved for bonding schemes, interaction energies, or charge distributions. Particularly in the area of organometallic complexes, where one is interested in catalytic activity, accurate knowledge of bond strengths, modes of bonding, charge distributions, force constants, and oxidation states is desirable. It is especially desirable to obtain the same data for a series of complexes or metals so that systematic errors which inevitably occur in any computational model will tend to cancel.

We have recently proposed a scheme within the HFS framework based on a transition-state method for the computation of bond energies.[6] The scheme naturally yields an analysis of the contributions to bond strengths in terms such as steric and electrostatic interaction and σ- and π-electron donation, which are in common parlance for simpler organic and inorganic systems. It also provides ready identification in PMO language of the fragment molecular orbitals which interact to form bonds and determine conformational preferences. Initial calculations on some diatomic molecules and a few transition-metal complexes gave results in better agreement with experiment than have yet been achieved by the Hartree–Fock method[6] (and with considerably less computational effort).

We present below a brief outline of the scheme presented in detail elsewhere[6] and then present a detailed analysis of the coordination between ethylene and the transition-metal ions or fragments Cu^+, Ag^+, Au^+, $PtCl_3^-$, and $Pt(PH_3)_2$.

2. Theory

2.1. Transition-State Method for the Calculation of Bonding Energies by the Hartree–Fock–Slater Method. Consider the molecule $\overline{\mathrm{AB}}$, with electronic density $\rho_{(AB)}$, where the subscript (AB) indicates that the molecule is formed from the two electronic systems (molecules) A and B with densities ρ_A and ρ_B, respectively. If the molecules A and B are described by the occupied and virtual orbitals $\{U_i^\alpha, U_i^\beta\}$ where α and β indicate electrons of spin up and spin down, then one might write

$$\rho_{AB} = \rho_A + \rho_B = \sum_i^{occ} P_{ii}^\alpha \cdot U_i^\alpha(\vec{r}_1) \cdot U_i^\alpha(\vec{r}_1) + \sum_i^{occ} P_{ii}^\beta \cdot U_i^\beta(\vec{r}_1) \cdot U_i^\beta(\vec{r}_1) \quad (2.1)$$

and

$$\rho_{(AB)} = \sum_{ij} (P_{ij}^\alpha \cdot \delta_{ij} + \Delta P_{ij}^\alpha) U_i^\alpha(\vec{r}_1) \cdot U_j^\alpha(\vec{r}_1) + \sum_{ij} (P_{ij}^\beta \cdot \delta_{ij} + \Delta P_{ij}^\beta) U_i^\beta(\vec{r}_1) \cdot U_j^\beta(\vec{r}_1) \quad (2.2)$$

where P_{ii} is the bond order matrix for $\rho_A + \rho_B$ (A and B at infinite separation) and $P_{ij} \cdot \delta_{ij} + \Delta P_{ij}$ the bond order matrix for $\rho_{(AB)}$, both with respect to the basis $\{U_i\}$.

Table I. Calculated Metal–Carbon Bond Distances and Bonding Energies for the Complex **1**, between Cu^+, Ag^+, and Au^+ and Ethylene

		energy contributions to the bonding energy,[a] au					
	R_{MC},[b] Å	E_{el}	$\Delta E°$	ΔE^{A_1}	ΔE^{B_1}	$\Delta E^{A_2} + E^{B_2}$	ΔE,[c] au
Cu^+–C_2H_4	1.95	−0.127	0.010	−0.049	−0.083	−0.005	−0.127
Ag^+–C_2H_4	2.40	−0.072	−0.021	−0.045	−0.010	−0.005	−0.080
Au^+–C_2H_4	2.47	−0.091	−0.032	−0.037	−0.010	−0.002	−0.080

[a] 1 atomic unit of energy = 627.7 kcal/mol. [b] Equilibrium metal–carbon distance. [c] Total bonding energy.

The transition-state expression[5] for the bonding energy[6] of $\overline{AB}$ (ΔE) with respect to A and B at infinite separation is given as

$$\Delta E = \Delta E_{el} + \Delta E_{ex}{}^{\alpha} + \Delta E_{ex}{}^{\beta} + \sum_{ij} F_{ij}{}^{\alpha} \cdot \Delta P_{ij}{}^{\alpha} + \sum_{ij} F_{ij}{}^{\beta} \cdot \Delta P_{ij}{}^{\beta} \quad (2.3)$$

where

$$\Delta E_{el} = \sum_{g_A}\sum_{g_B} Z_{g_A} Z_{g_B} / |\vec{R}_{g_A} - \vec{R}_{g_B}| + \int \rho_A(\vec{r}_1)\rho_B(\vec{r}_2)/r_{12}\, d\vec{r}_1\, d\vec{r}_2 - \sum_{g_A} \int \rho_B(r_1) Z_{g_A} / |\vec{r}_1 - \vec{R}_{g_A}|\, d\vec{r}_1 - \sum_{g_B} \int \rho_A(r_1) Z_{g_B} / |\vec{r}_1 - \vec{R}_{g_B}|\, d\vec{r}_1 \quad (2.4)$$

is the electrostatic interaction between molecules A and B, and

$$\Delta E_{ex}{}^{\alpha} = -(3/4) \int \rho_A{}^{\alpha}(\vec{r}_1) V_{HFS}{}^{\alpha}(\rho^{\alpha}(\vec{r}_1))\, d\vec{r}_1 - (3/4) \int \rho^{\alpha}(\vec{r}_1) V_{HFS}{}^{\alpha}(\rho_B{}^{\alpha}(\vec{r}_1))\, d\vec{r}_1 + (3/4) \int \rho_{AB}{}^{\alpha}(\vec{r}_1) V_{HFS}{}^{\alpha}(\rho_{AB}{}^{\alpha}(\vec{r}_1))\, d\vec{r}_1 \quad (2.5)$$

$$\sum_{ij} F_{ij}{}^{\alpha} \cdot \Delta P_{ij} = \sum_{ij} \Big\{ 2/3 \cdot \int U_i{}^{\alpha}(\vec{r}_1) h^{\alpha}((1/2)\{\rho_{AB} + \rho_{(AB)}\}) U_j{}^{\alpha}(\vec{r}_1)\, d\vec{r}_1 + 1/6 \cdot \int U_i{}^{\alpha}(\vec{r}_1) h^{\alpha}(\rho_A) U_j{}^{\alpha}(\vec{r}_1) \int d\vec{r}_1 + (1/6) \int U_i{}^{\alpha}(\vec{r}_1) h^{\alpha}(\rho_B) U_j(\vec{r}_1)\, d\vec{r}_1 \Big\} \cdot \Delta P_{ij}{}^{\alpha} \quad (2.6)$$

with a similar expression for $\sum_{ij} F_{ij}{}^{\beta} \cdot \Delta P_{ij}{}^{\beta}$. Here $\rho_{AB} = \rho_A + \rho_B$ and $h^{\alpha}(\rho)$ is the one-electron HFS operator given by

$$h^{\alpha}(\rho) = f(\vec{r}_1) + \int \rho(X_2)/r_{12}\, dX_2 + V_{HFS}{}^{\alpha}(\rho^{\alpha}) \quad (2.7)$$

where $f(\vec{r}_1)$ is the sum of the operators for the kinetic energy of an electron and the attraction energy between an electron and the nuclei. The indices in i, j in eq 2.6 run over both occupied and virtual orbitals of A and B. The matrix element F_{ij} is clearly a function of ρ_A, ρ_B, and $\rho_{(AB)}$ and this will later on be indicated by writing the matrix element as $F_{ij}(\rho_A, \rho_B, \rho_{(AB)})$.

The total bonding energy ΔE is divided up into a steric part, $\Delta E°$, and an electronic part, $\sum_{\Gamma} \Delta E^{\Gamma}$, where Γ runs over all symmetry representations in the symmetry point group of $\overline{AB}$. The steric part, $\Delta E°$, is the bonding energy of $\overline{AB}$ from a calculation in which only occupied orbitals on A and B are used. Let the total density from such a calculation be given by

$$\rho_{(AB)}{}° = \sum_{ij} U_i(\vec{r}) U_j(\vec{r}) \cdot \{P_{ij}{}° \cdot \delta_{ij} + \Delta P_{ij}{}°\} \quad (2.8)$$

Then

$$\Delta E° = \Delta E_{ex} + \Delta E_{el} + \sum_{ij}^{occ} F_{ij}(\rho_A, \rho_B, \rho_{(AB)}{}°) \Delta P_{ij}{}° \quad (2.9)$$

where the sum of the first and last terms in eq 2.9 later on will be referred to as the exchange repulsion, ΔE_{er}. The steric interaction, $\Delta E°$, is the energy of interaction when neither system can change in response to the presence of the other and no electron transfer can take place. It may be attractive or repulsive.

The electronic part of the bonding energy, $\sum_{\Gamma} E^{\Gamma}$, arises when we include the virtual orbitals on A and B in the calculation and is given by

$$\Delta E^{\Gamma} = \sum_{ij} F_{ij,\Gamma}(\rho_A, \rho_B, \rho_{(AB)}) \cdot \Delta P_{ij,\Gamma} - \sum_{ij}^{occ} F_{ij,\Gamma}(\rho_A, \rho_B, \rho_{(AB)}{}°) \Delta P_{ij,\Gamma}{}° \quad (2.10)$$

Here the indices i and j run over all spin orbitals which transform as the irreducible representation Γ and $\rho_{(AB)}$ is the electron density of molecule $\overline{AB}$ with corresponding P matrix $\{P_{ij} \cdot \delta_{ij} + \Delta P_{ij}\}$. The electronic part of the bond energy accounts for the response of one system to the presence of the other and yields the donor–acceptor interactions that occur between them. Equation 2.10 gives a direct connection between bond orders and bond energies.

The decomposition scheme outlined in this section is in outlook closely related to the work of Fujimoto and Fukui[7] as well as Kitaura and Morokuma.[8] An interesting decomposition scheme based on perturbational molecular orbital theory has recently been published by Whangbo, Schlegel, and Wolfe.[9]

2.2. Computational Details. The geometries of $Pt(Cl)_3^-$–C_2H_4 and $Pt(PH_3)_2$–C_2H_4 were taken from ref 10 and 11, respectively.

Core orbitals were kept frozen according to the procedure by Baerends et al.[12] The valence orbitals were represented by a double-ζ Slater basis set optimized with respect to the total ground-state energies of the respective atoms. A third d component was added in the molecular calculations to the basis of each metal and a single d component ($z = 1.3$) to the P basis. A value of 0.7 was used for the exchange parameter α in all calculations. Relativistic effects were completely neglected.

3. Bonding Analysis

3.1. Ethylene Complexes of Cu^+, Ag^+, and Au^+. The various terms introduced in section 2.1 will now be illustrated in connection with an analysis of the bonding in the M(+)–ethylene complex, **1**. The metal ion (Cu^+, Ag^+, Au^+) is

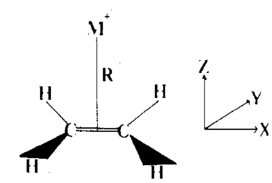

1

situated above the center of the olefin double bond at a distance R.

3.2. Steric Interaction Energy, $\Delta E°$, in Cu^+–C_2H_4, Ag^+–C_2H_4, and Au^+–C_2H_4. The two factors that make up the steric interaction energy (ΔE_{el} and ΔE_{er}) are shown as a function of ion–olefin separation, R, in Figures 1 and 2, respectively. The electrostatic interaction, ΔE_{el}, not surprisingly, is attractive due to the net positive charge on the metal. However, a comparison with the electrostatic interaction between a proton

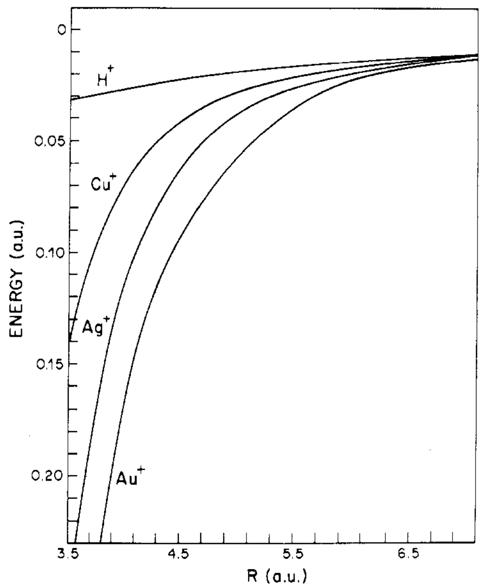

Figure 1. Electrostatic interaction energy, ΔE_{el}, between H^+, Cu^+, Ag^+, or Au^+ and ethylene, as a function of R.

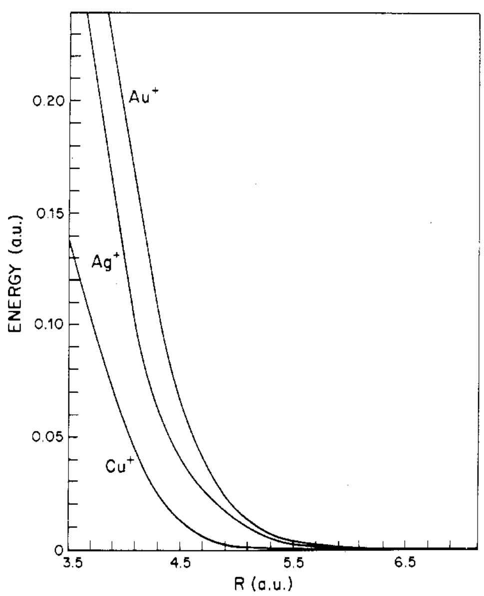

Figure 2. Exchange repulsion energy, ΔE_{er}, between Cu^+, Ag^+, or Au^+ and ethylene as a function of R.

and ethylene, Figure 1, shows that the net positive charge only partly accounts for the attraction. An additional contribution stems from the penetration of the metal electrons beyond the screening effect of the olefin electrons and the penetration of the ethylene electrons beyond the screening effect of the metal electron cloud. The penetration becomes increasingly important toward smaller values of R and, as is shown in Figure 1, most important for the metal ion Au^+, with the most diffuse electron cloud and highest nuclear charge.

The exchange repulsion term, ΔE_{er}, for the three olefin complexes is shown in Figure 2 as a function of R. The major part of ΔE_{er} comes from the interaction between the occupied (n)s, $(n)p_z$, and $(n)d_{z^2}$ orbitals on the metal and the occupied π orbitals on ethylene. The interaction due to exchange repulsion is illustrated in Figure 3a for the system Cu^+–C_2H_4 by means of a density difference map between $\rho_A + \rho_B$, the sum of the densities of M^+ and ethylene, and the resulting density from a calculation on the combined complex involving only the occupied orbitals of M^+ and ethylene. Electron density is removed from the area where the π olefin orbital

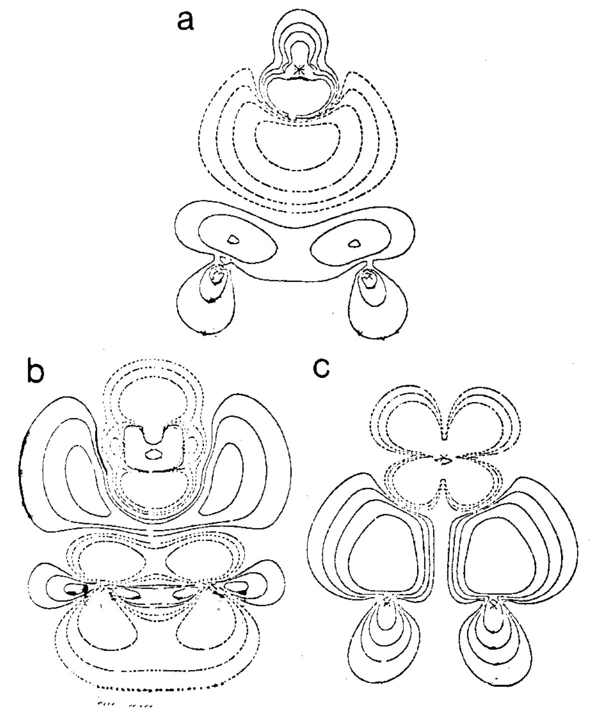

Figure 3. Electron density difference maps. Figure 3a represents $\rho_1 - \rho_2$, where ρ_2 is the sum of the densities from all occupied orbitals on Cu^+ and C_2H_4 and ρ_1 is the total density of the combined complex from a calculation in which only the occupied orbitals on Cu^+ and C_2H_4 have been used. Figure 3b represents $\rho_3 - \rho_4$, where ρ_3 is the sum of the densities of all occupied orbitals on Cu^+ and C_2H_4 transforming as A_1 in the C_{2v} symmetry group and ρ_4 is the sum of the densities of all occupied orbitals in the combined complex transforming as A_1. Figure 3c represents $\rho_5 - \rho_6$, where ρ_5 is the sum of the densities of all occupied orbitals on Cu^+ and C_2H_4 transforming as B_1 in the C_{2v} symmetry group and ρ_6 is the sum of the densities of all occupied orbitals in the combined complex transforming as B_1. Contours: 0.1, 0.05, 0.025, 0.01. Dashed contours represent regions of decreased electron density.

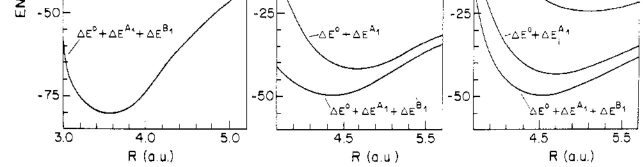

Figure 4. Decomposition of the bonding energy of Cu^+–C_2H_4, Ag^+–C_2H_4, and Au^+–C_2H_4 into the steric energy, $\Delta E°$, and the contributions from the σ donation, ΔE^{A_1}, and π back-donation, ΔE^{B_1}. The contributions from the A_2 and B_2 representations (both small) have been absorbed into $\Delta E° + \Delta E^{A_1}$ for clarity. The absolute values of those terms are given in Table I for $R = R_e$.

overlaps with the (n)s, $(n)p_z$, and $(n)d_{z^2}$ metal orbitals. For any distance, R, the exchange repulsion is most important for Au^+, the metal ion with the most diffuse electron cloud. It becomes the dominant term in the expression of $\Delta E°$ (eq 2.9) toward smaller values of R.

The sum of ΔE_{el} and ΔE_{er}, $\Delta E°$, which is the total steric interaction energy, is shown in Figure 4 for the three olefin

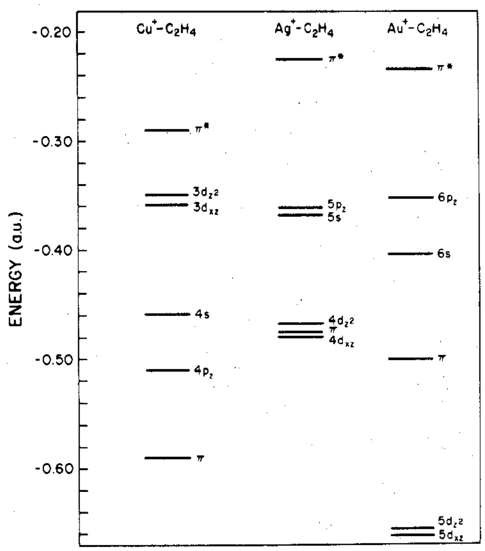

Figure 5. Orbital energies of Cu^+, Ag^+, or Au^+ and C_2H_4 in the combined complexes. The orbital energies of C_2H_4 include the electrostatic energy and exchange energy due to the metal ion (and vice versa).

complexes. In each case, the steric interaction energy alone has a minimum but overestimates the metal–olefin separation and underestimates the binding energy.

3.3. Donation and Back-Donation. The bonding between the d^{10} metal ions Cu^+, Ag^+, and Au^+ and ethylene is explained, in terms of modern molecular orbital theory, as a synergic[13] donor–acceptor process. Electrons are donated from the π olefin orbital to the virtual $(n+1)$s orbital on the metal **2**, and at the same time a back-donation takes place from the $(n)d_{xz}$ metal orbital to the empty π^* olefin orbital **3**.

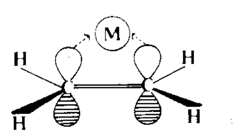

2

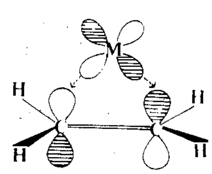

3

The energy contributions corresponding to **2** (σ donation) and **3** (π back-donation) are ΔE^{A_1} and ΔE^{B_1}, respectively, in our decomposition scheme for the bonding energy, ΔE. Figure 4 shows the different energy contributions $\Delta E°$, ΔE^{A_1}, and ΔE^{B_1} for the three olefin complexes as a function R.

It follows from the figure that ΔE^{A_1} is important for all three complexes and the dominant factor for Ag^+–C_2H_4 and Au^+–C_2H_4. ΔE^{A_1} has a sizable contribution to the bonding energy even at values of R much larger than the equilibrium distance R_e. This is understandable since the donation involves the rather diffuse $(n+1)$s orbital. The back-donation, ΔE^{B_1}, is very important for Cu^+–C_2H_4 but less important for Ag^+–C_2H_4 and $Au^+C_2H_4$. The back-donation has only small contributions at distances larger than R_e and increases markedly in importance toward smaller values of R. The short range effect of ΔE^{B_1} stems from the fact that it is a function of the interaction between the two relatively contracted orbitals π^* and $(n)d_{xz}$.

The relative importance of donation and back-donation in the three olefin complexes is readily understood in simple PMO terms from Figure 5 where the energies of the metal and ethylene orbitals "in the complex" are compared. The orbital energy of U_i "in the complex" is defined as

$$E_{U_i} = \int U_i(X_1)\{h^\alpha(\rho_A + \rho_B) + h^\beta(\rho_A + \rho_B)\}U_i(X_1)\,dX_1 \tag{3.1}$$

Table II. Mulliken Population Analysis of Cu^+-C_2H_4, Ag^+-C_2H_4, and Au^+-C_2H_4 in Terms of the Ethylene Orbitals and the Orbitals of the Free Ions

orbital	Cu^+-C_2H_4	Ag^+-C_2H_4	Au^+-C_2H_4
d_{z^2}	1.89	1.94	2.00
π	1.68	1.77	1.89
d_{xz}	1.73	1.95	1.97
$(n+1)$s	0.40	0.22	0.11
$(n+1)p_z$	0.00	0.05	0.03
π^*	0.25	0.05	0.03

where ρ_A and ρ_B are the densities of ethylene and the metal ion, respectively. The $(n+1)$s metal orbital olefin π orbital energy separation is similar for all three complexes, and thus donation should be of the same importance in Cu^+–C_2H_4, Ag^+–C_2H_4, and Au^+–C_2H_4. In the case of back-donation, only the $(n)d_{xz}$ orbital on Cu^+ has an energy comparable to that of π^* on ethylene. As a result ΔE^{B_1} is more important for Cu^+–C_2H_4 than for Ag^+–C_2H_4 or Au^+–C_2H_4. The energies of the d orbitals shown in Figure 5 contain exchange and electrostatic contributions (both stabilizing) from ethylene. The contributions are most important for the metal ion, Au^+, with the most diffuse d orbital.

A Mulliken population analysis in terms of the ethylene molecular orbitals and the atomic orbitals of the free ions is shown in Table II. The analysis confirms that the ethylene to metal electron donation takes place mainly from the olefin π orbital to the $(n+1)$s orbital on the metal. In addition, the $(n+1)$s orbital serves to remove charge (polarization) from the d_{z^2} orbital in order to reduce the four-electron destabilizing interaction between d_{z^2} and π (see Figure 3a). An electron density difference map of the donation process is shown in Figure 3b. The analysis in Table II shows that the back-donation of electrons from the metal to the olefin mainly involves the d_{xz} and π^* orbitals. The back-donation process is illustrated in Figure 3c.

That the bonding descriptions given above are realistic may be verified by comparing calculated bond separations and dissociation energies. Numerous X-ray crystal structure examinations have been reported on Cu^+ and Ag^+ olefin complexes[13] in which the metal ion is coordinated to one double bond. The metal–carbon distance R_{MC} falls in the range 1.97–2.11 Å for silver complexes, in good agreement with the calculated R_{MC} values given in Table I.

Dissociation energies are more difficult to evaluate. The energy of formation, $-\Delta E_1$, for the process

$$M^+ + C_2H_4 \rightarrow M^+\text{–}C_2H_4 \tag{3.2}$$

where a positive value for $-\Delta E_1$ indicates that the complex is stable with respect to its components, is not known experimentally. A number of $-\Delta E_2$ values[11] have been reported for the process

$$A^-(aq) + Aq^+(aq) + C_2H_4(aq) \rightarrow A^-(aq) + Ag^+\text{–}C_2H_4(aq) \tag{3.3}$$

and occur in the range between 7 and 10 kcal, depending on A^-. In order to obtain $-\Delta E_1$ from experiment one would have to add to $-\Delta E_2$ the energy $(-\Delta E_3)$ required to remove one or more water molecules from the coordination sphere of Ag^+. This energy is not known experimentally, but a lower limit value to $-\Delta E_3$ would be the enthalpy of activation for the process 3.3, known[15] to be 20 kcal for $A^- = ClO_4^-$. Thus a lower limit estimate of $-\Delta E_1$ would be 30 kcal, compared to the calculated value of 50 kcal, in Table I.

There have been several semiempirical treatments[16] of complexes between Cu^+, Ag^+, and Au^+ and various olefins as well as a HF–SCF ab initio calculation on Ag^+–C_2H_4 by Basch.[17] The accuracy of the semiempirical methods is difficult to assess; however, the results of Basch[17] regarding

Table III. Decomposition of the Bonding Energy of Zeise's Salt $PtCl_3^-$–C_2H_4 in the Two Conformations

conformations	energies,[a] au						
	E_{el}	E_{er}	$\Delta E°$	ΔE^{A_1}	ΔE^{B_1}	ΔE^{B_2}	ΔE
4	−0.308	0.425	0.118	−0.077	−0.056	0.004	−0.023
5	−0.277	0.360	0.084	−0.068	−0.003	−0.054	−0.044

[a] $\Delta E^{A_2} = -0.012$ and -0.009 for **4** and **5**, respectively.

the relative importance of σ donation and π back-donation for Ag^+–C_2H_4 are in qualitative agreement with the present work.

4. Conformation Analysis

4.1. Conformation of Ethylene in $Pt(Cl)_3^-$–C_2H_4 and $Pt(PH_3)_2$–C_2H_4. Several X-ray diffraction measurements[10,18] on Zeise's anion, $Pt(Cl)_3^-$–C_2H_4, show ethylene perpendicular to the coordination plane of $PtCl_3^-$, **5**, rather than in the plane, **4**. The same conformation is observed in other d^8 platinum

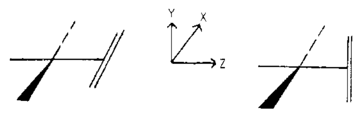

4 **5**

complexes[19] with C_2H_4, where one or more chlorines have been substituted by other ligands. The d^{10} platinum complexes with ethylene, of the type $Pt(L)_2$–C_2H_4, where L might be a phosphine or isocyanide, show[20] ethylene in the coordination plane of $Pt(L)_2$, **6**, rather than perpendicular to the plane, **7**.

6 **7**

The observed structures of Zeise's salt and of $Pt(PH_3)_2$–C_2H_4 have been rationalized by application of simple perturbation theory to the results of semiempirical calculations based on extended Hückel theory.[1,22] Both systems have also been examined by the MS-Xα method.[11,23] However, bonding energies or energies due to σ donation and π back-donation were not reported.

An evaluation will now be given of the importance of the steric interaction, $\Delta E°$, as well as the σ donation and π back-donation for the coordination of ethylene in the d^8 and d^{10} platinum complexes.

4.2. Relative Stability of Conformation 5 Compared to 4. The bonding energy ΔE between $PtCl_3^-$ and C_2H_4 is shown in the last column of Table III for configuration **4** as well as **5**. A negative value for ΔE indicates that the complex is stable with respect to the two components $PtCl_3^-$ and C_2H_4. The bonding energies have been decomposed according to the scheme outlined in section 2.1.

It is clear from Table III that configuration **5** has a lower energy than **4** primarily due to the steric factor $\Delta E°$ $(=\Delta E_{el} + \Delta E_{er})$, whereas the electronic effect $(E^{A_1} + E^{B_1} + E^{B_2})$ plays a minor role for the relative stability of **4** compared to **5**. A more detailed analysis will now be given in connection with the data presented in Figure 6 in which are shown the energy for the molecular orbitals of $PtCl_3^-$ and C_2H_4 "in the combined complex" and also the shapes of some of the important orbitals of the two fragments.

We begin by discussing the steric interaction energy, $\Delta E°$, of the two conformations of Zeise's salt. The positive and thus destabilizing part of $\Delta E°$ comes from the repulsive interaction between occupied orbitals on $PtCl_3^-$ and C_2H_4. Parts of each of the occupied orbitals on $PtCl_3^-$ are located on the metal and give rise to strong repulsive interactions with the occupied orbitals on ethylene, in particular with $1a_{1g}$, $2a_1$g, and π (Figure 6). The metal charge on $PtCl_3^-$ is, to a good ap-

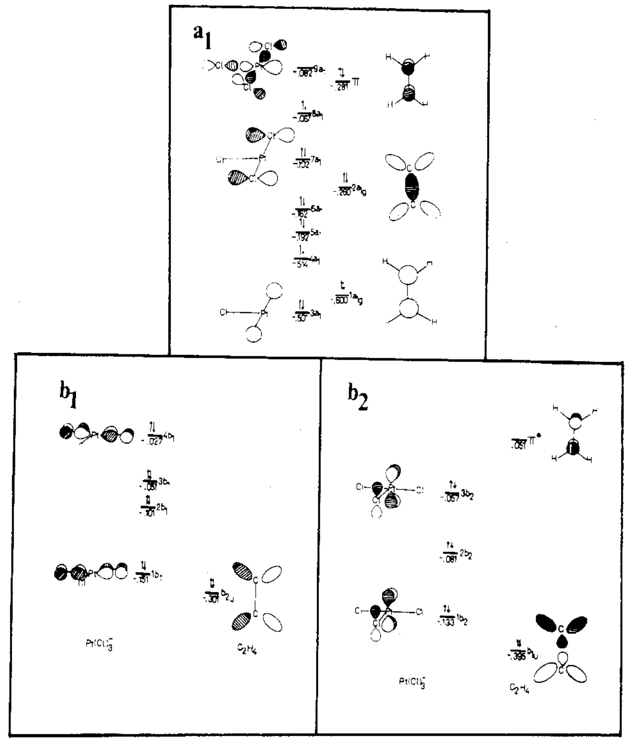

Figure 6. Orbital energies of $PtCl_3^-$ and C_2H_4 in the combined complex. Also shown are the shapes of some of the important orbitals on $PtCl_3^-$ and C_2H_4.

proximation, symmetrical with respect to any rotation around the z axis according to the present HFS calculation. Thus a rotation of ethylene around the same axis from **4** to **5** does not change the exchange repulsion due to the metal–ethylene interaction.

The distances between the chlorines cis to ethylene and the carbons on ethylene or between the same chlorines and the ethylene hydrogens are somewhat smaller in Zeise's salt when ethylene is placed in the coordination plane of $PtCl_3^-$ rather than perpendicular to the plane. The parts of the occupied orbitals of $PtCl_3^-$ localized on the two chlorines cis to C_2H_4 will as a consequence interact more strongly with the occupied orbitals to ethylene in conformation **4** than in conformation **5**. This effect is particularly important for the interaction between $3a_1$, $7a_1$ on $PtCl_3^-$ and $1a_{1g}$, π on ethylene (Figure 6, a_1). A final point of interest for the analysis of $\Delta E°$ is the interaction between $2a_{1g}$ on ethylene and $3a_1$, $7a_1$ on $PtCl_3^-$. The ethylene orbital ($2a_{1g}$) has two nodal planes (Figure 6, a_1). In conformation **4** where C_2H_4 is in the coordination plane of $PtCl_3^-$, only positive parts of $2a_{1g}$ interact with $3a_1$ and $7a_1$. When ethylene is in its upright position (conformation **5**), both negative and positive parts of $2a_{1g}$ interact with $3a_1$, $7a_1$. The cancellation of positive and negative contributions results in a smaller repulsive interaction between $2a_{1g}$ and $7a_1$, $3a_1$ for this orientation of ethylene, and thus adds to the overall stability of conformation **5** compared to conformation **4**.

4.3. σ Donation in $Pt(Cl)_3^-$–C_2H_4. The σ donation is described in the classical Dewar–Chatt–Duncanson[13,21] model as a transfer of charge from the π orbital on ethylene to an orbital on the metal with s,p,d character. According to the

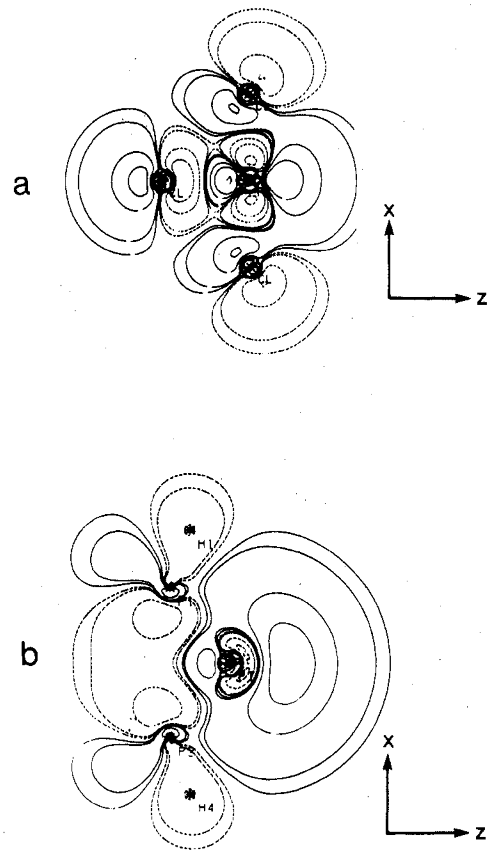

Figure 7. Contour diagram of $9a_1$ on $PtCl_3^-$ and $8a_1$ on $Pt(PH_3)_2$. Figure 7a shows $9a_1$ in the *xz* plane. Figure 7b shows $8a_1$ in the same plane. Contour values: 0.25, 0.1, 0.05, 0.01, 0.005. Dotted lines represent negative contours, that is, regions of decreased electron density.

Table IV. Mulliken Population Analyses of Zeise's Salt over the Orbitals of C_2H_4 and $PtCl_3^-$ in the Two Conformations

conformations	populations							
	$7a_1$	$9a_1$	π	$1b_1$	$4b_1$	$1b_2$	$3b_2$	π^*
4	1.80	0.58	1.64	1.86	1.90	2.00	2.00	0.26
5	1.88	0.46	1.66	2.00	2.00	1.90	1.84	0.27

present calculation the charge is primarily donated to $9a_1$ (Figure 6), the lowest unoccupied orbital on $PtCl_3^-$. This orbital, displayed as a contour map in Figure 7a, is an antibonding combination between p orbitals on the three chlorines and a hybrid platinum orbital of 6s, 6p, and 5d character. The σ donation is illustrated in Figure 8, for conformation **5**, by three electron-density difference maps drawn in the *xz*, *yz*, and *xy* planes, respectively. The maps illustrate the difference between the sum of the densities (ρ_1) of all occupied orbitals on $PtCl_3^-$ and C_2H_4 transforming as a_1 in the C_{2v} point group and the sum of the densities (ρ_2) of all occupied orbitals with a_1 symmetry in the combined complex. The maps correspond to the difference $\rho_2 - \rho_1$. The dotted lines represent areas where charge has been removed on complex formation and solid line areas where charge has been added.

The gross picture of the σ donation involves the occupied π orbital on C_2H_4 and the occupied and virtual orbitals $7a_1$ and $9a_1$ on $PtCl_3^-$. The occupation of these orbitals from Mulliken population analysis on Zeise's salt in the two conformations are given in Table IV. The interaction (Figure 8a) results in a rehybridization around the two chlorines cis to ethylene which may be viewed as a promotion of electrons from $7a_1$ to $9a_1$. This rehybridization reduces somewhat the exchange repulsion between the two cis chlorines and ethylene.

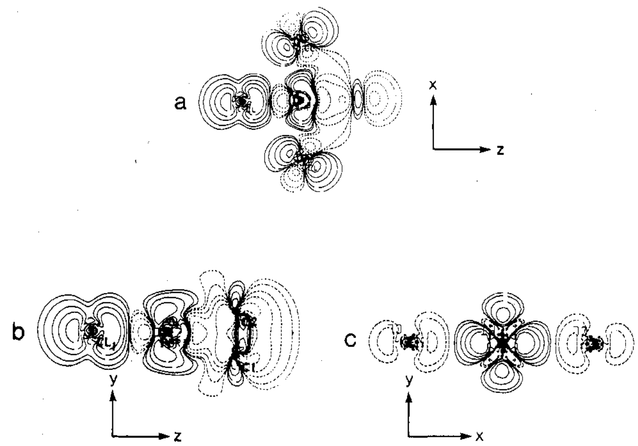

Figure 8. Electron density difference maps of donation in Zeise's salt. The difference is between the density (ρ_1) due to the sum of all occupied orbitals on $PtCl_3^-$ and C_2H_4 transforming as a_1 in the C_{2v} point group and the density (ρ_2) due to the sum of all occupied orbitals of a_1 symmetry in the combined complex. The difference $\rho_2 - \rho_1$ is depicted in diagrams a, b, and c in the *xz*, *yz*, and *xy* planes, respectively. The contour values: 0.25, 0.1, 0.05, 0.025, 0.01, 0.005, 0.001, and 0.0005. Dotted lines represent negative values, that is, regions of decreased electron density.

The direct donation from π on ethylene to $9a_1$ on $PtCl_3^-$ has a similar energetic effect. Charge is removed from between the two fragments and the exchange repulsion reduced between Pt and C_2H_4. The maps in Figure 8 show that most of the charge is donated to the three chlorines. However, some density is built up around the metal along the *x* and *y* axes.

The energy due to the σ donation is given in Table III as ΔE^{A_1}.

4.4. π Back-Donation in Zeise's Salt. The π back-donation in conformation **5** involves $1b_2$ and $3b_2$ on $PtCl_3^-$, both occupied, as well as the virtual π^* orbital on C_2H_4; see Figure 6. The energy due to the π back-donation is given in Table III as ΔE^{B_2} for conformation **5**. The two donor orbitals in conformaton **4** are $1b_1$, $4b_1$ (Figure 6) and the energy due to π back-donation in this conformation is given in Table III as ΔE^{B_1}. The two energies are rather close and show that π back-donation is of little importance for determining the relative stabilities of **4** and **5**.

The fact that the difference between ΔE^{B_1} and ΔE^{B_2} is small is related to the close similarity between $1b_1$, $1b_2$ and between $4b_1$, $3b_2$, as donor orbitals. The orbitals $1b_1$ and $1b_2$ both originate from a weak π-bonding interaction between d orbitals on Pt and lone pairs on the chlorines (Figure 6). The result is two orbitals of roughly the same energy relative to π^* and both with similar shapes for suitable overlaps with π^*. The two orbitals $4b_1$ and $3b_2$ are the corresponding antibonding combinations again with roughly the same energies relative to π^* and both of similar suitable shapes for overlaps with π^* (Figure 6). The back-donation process is depicted in Figure 9 by a density difference map with ethylene in conformation **5**. Charge is donated (dotted lines) from $5d_{yz}$ on Pt to π^* on C_2H_4 (solid lines).

The occupations of $1b_2$, $3b_2$ and π^* from a Mulliken population analysis on Zeise's salt for both conformations are given in Table IV.

4.5. Bonding Energies for $Pt(PH_3)_2$–C_2H_4 in Conformation 6 and Conformation 7. The bonding energies, ΔE, for $Pt(PH_3)_2$–C_2H_4 in conformation **6** and conformation **7** are given in Table V. A close inspection of the table shows that the steric interaction energy $\Delta E°$ and the energy due to the σ donation from C_2H_4 to $Pt(PH_3)_2$, given as ΔE^{A_1}, are of little importance for the relative stability of conformation **6** compared to conformation **7**. The energy due the π back-donation is given as ΔE^{B_1} for conformation **6** and as ΔE^{B_2} for

Table V. Decomposition of the Bonding Energy of $Pt(PH_3)_2$–C_2H_4 in the Two Conformations

conformations	bonding energies,[a] au						
	E_{el}	E_{er}	ΔE°	ΔE^{A_1}	ΔE^{B_1}	ΔE^{B_2}	ΔE
6	−0.186	0.212	0.026	−0.023	−0.056	−0.004	−0.057
7	−0.183	0.208	0.025	−0.023	−0.004	−0.046	−0.048

[a] There are no significant contributions from ΔE^{A_2}.

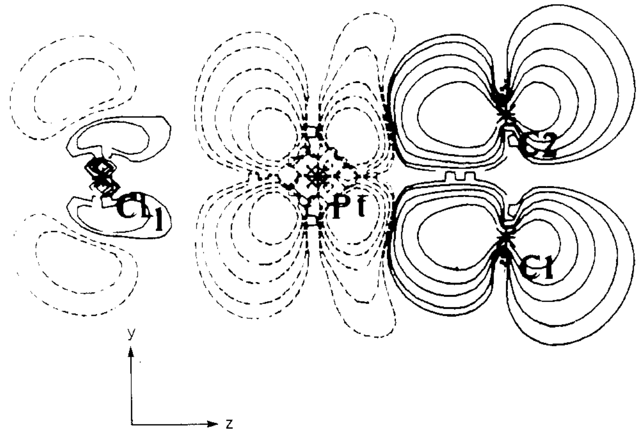

Figure 9. Electron difference map of back-donation in Zeise's salt. The difference is between the density (ρ_1) due to the sum of all occupied orbitals of $PtCl_3^-$ and C_2H_4 transforming as b_2 in the C_{2v} point group and the density (ρ_2) due to the sum of all occupied orbitals of b_2 symmetry in the combined complex. The difference $\rho_2 - \rho_1$ is depicted in the *yz* plane. Contour values: 0.25, 0.1, 0.05, 0.025, 0.01, 0.005, 0.001, and 0.0005. Dotted lines represent negative values, that is, regions of decreased electron density.

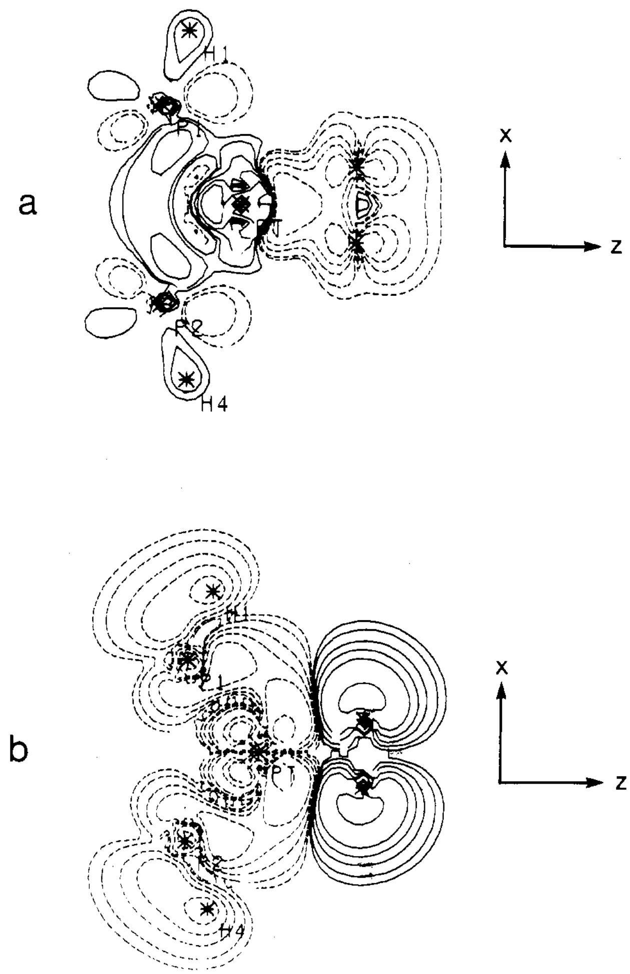

Figure 10. Electron density difference map of σ donation, plot a, and π back-donation, plot b, in $Pt(PH_3)_2$–C_2H_4 and C_2H_4 transforming as a_1 (plot a) or b_1 (plot b) in the C_{2v} point group and the density (ρ_2) due to the sum of all occupied orbitals of A_1, plot a, or B_1, plot b, symmetry in the combined complex. The difference $\rho_2 - \rho_1$ is depicted in the *xz* plane. Contour values: 0.25, 0.1, 0.05, 0.025, 0.01, 0.005, 0.001, 0.0005. Dotted lines represent negative values, that is, regions of decreased electron density.

conformation **7**. The table shows that conformation **6** is more stable than conformation **7** due to the π back-donation.

The portions of the occupied orbitals from the $Pt(PH_3)_2$ fragment that are located on the PH_3 ligands do not overlap with the occupied orbitals on ethylene in either of the conformations. As a consequence, the exchange repulsion is due to the overlap between the occupied ethylene orbitals and the portions of the occupied orbitals from the $Pt(PH_3)_2$ fragment located on the metal. However, the exchange repulsion does not change appreciably when ethylene is rotated around the *z* axis since the density on Pt is almost cyllindrical around the same axis.

The two orbitals of importance for σ donation are π on ethylene and the lowest unoccupied orbital on $Pt(PH_3)_2$, $8a_1$. A contour map of $8a_1$ is shown in Figure 7b. The parts of $8a_1$ of importance for the overlap with the π orbital are on the metal and consist of 6s, $6p_z$, $5d_{z^2}$ hybrid. The rotation symmetry of this hybrid around the *z* axis makes it understandable that σ donation is of the same importance in both conformations.

A density difference map of the σ donation is given in Figure 10a, and the occupations of π and $8a_1$ from a Mulliken population analysis can be seen in Table VI.

4.6. π Back-Donation in $Pt(PH_3)_2$–C_2H_4. The electronic density donated to π^* on ethylene comes from $1b_1$, $2b_1$ on $Pt(PH_3)_2$ in conformation **6** and from $1b_2$ on $Pt(PH_3)_2$ in conformation **7**. The shapes and orbital energies of $1b_1$, $2b_1$, and $1b_2$ are shown in Figure 11. The energies are in the order expected for bonding ($1b_1$), nonbonding ($1b_2$), and antibonding ($2b_1$) orbitals.

The energy difference favoring conformation **6** over **7** may be understood in simple PMO terms after considering the shapes and energies of the orbitals involved in the principal interactions $2b_1$–π^* and $1b_2$–π^*, respectively. In simple PMO theory, the magnitude of the stabilizing interaction is approximately proportional to the square of the overlap of the interacting orbitals and inversely proportional to the difference in their energies. The $2b_1$ orbital is higher in energy (and, therefore, closer to the π^* orbital of ethylene) than $1b_2$ because it is an antibonding combination of the metal $5d_{xz}$ orbital and the phosphorus lone pairs of the PH_3 ligands. Admixture of the $6p_x$ orbital of the metal serves to reduce the antibonding character of this orbital, as shown in structure **8**. This ad-

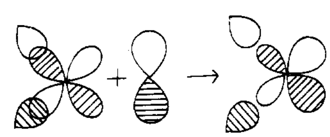

8

mixture in turn polarizes the $5d_{xz}$ orbital toward the ethylene thus leading to better overlap than is possible for the unpolarized $5d_{yz}$ ($1b_2$) orbital.

Mulliken population analyses for the molecular orbitals

Table VI. Mulliken Population Analyses of $Pt(PH_3)_2$–C_2H_4 over the Molecular Orbitals on C_2H_4 and $Pt(PH_3)_2$ in the Two Conformations

confor-mation	populations					
	$8a_1$	π	$1b_1$	$2b_1$	$1b_2$	π^*
6	0.20	1.82	1.96	1.60	2.00	0.43
7	0.18	1.84	2.00	2.00	1.76	0.21

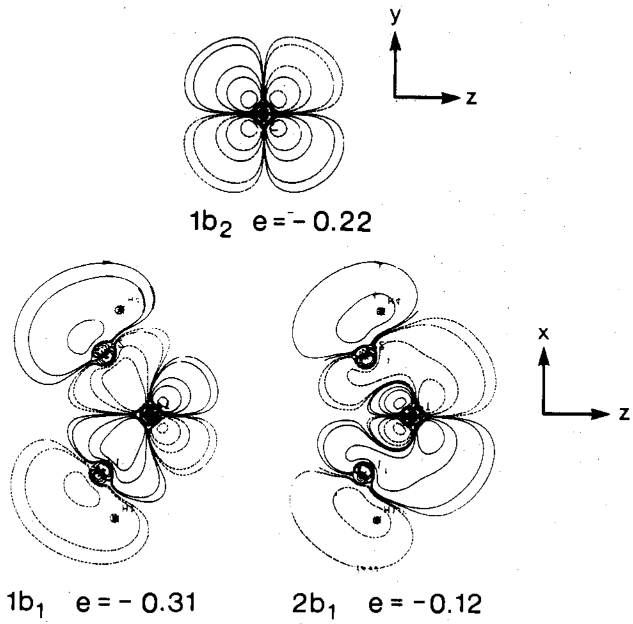

Figure 11. Shapes and orbital energies (in combined complex) of $1b_1$, $2b_1$, and $1b_2$. The orbital energy of π^* in the combined complex is –0.12 au.

involved in the two conformations confirm the descriptive account presented above and show a larger charge transfer from $2b_1$ to π^* in conformation **6** than from $1b_2$ to π^* in conformation **7**. The extent of the charge transfer in the former case (**6**) is graphically illustrated by the electron density difference map shown in Figure 10b.

In summary, the preferred conformation of ethylene in the d^8 system, Zeise's salt, $PtCl_3^-$–C_2H_4, in which the double bond is perpendicular to the $PtCl_3^-$ plane, **5**, arises largely as a consequence of dominant steric repulsions which are minimized in this conformation. The steric effects outweigh the bonding interactions, σ donation and π back-donation, both of which are more favorable for the in-plane conformation **4**. In the d^{10} system $Pt(CH_3)_2$–C_2H_4, the planar conformation **6** is preferred as a consequence of more favorable π back-donation. The steric interaction and σ donation are energetically very similar for the two conformations **6** and **7**.

Conclusions similar to ours have been developed independently by Hoffmann and co-workers[1] and by Norman.[11]

Acknowledgment. We wish to thank the National Research Council of Canada for support and the University of Calgary for the receipt of a generous computing grant. We also thank T. A. Albright, R. Hoffmann, J.C. Thibeault, and D. L. Thorn for communicating their results on $Pt(Cl)_3^-$–C_2H_4 and $Pt(PH_3)_2$ prior to publication.[1]

Registry No. Cu^+-C_2H_4, 60203-82-9; Ag^+-C_2H_4, 35827-90-8; Au^+-C_2H_4, 69596-89-0; $PtCl_3^-$-C_2H_4, 12275-00-2; $Pt(PH_3)_2$-C_2H_4, 31941-73-8.

References and Notes

(1) T. A. Albright, R. Hoffmann, J. C. Thibeault, and D. L. Thorn, in press, and references therein.
(2) J. C. Slater, *Adv. Quantum Chem.*, **6**, 1 (1972).
(3) J. W. D. Connolly, in "Modern Theoretical Chemistry", Vol. 7A, G. A. Segal, Ed., Plenum Press, New York, 1977, p 105.
(4) E. J. Baerends and P. Ros, *Int. J. Quantum Chem., Symp.*, **No. 12**, in press.
(5) K. H. Johnson, *Adv. Quantum Chem.*, **7**, 143 (1973).
(6) T. Ziegler and A. Rauk, *Theor. Chim. Acta*, **46**, 1 (1977).
(7) H. Fujimoto and K. Fukui, *Adv. Quantum Chem.*, **6**, 177 (1972).
(8) K. Kitaura and K. Morokuma, *Int. J. Quantum Chem.*, **10**, 325 (1976).
(9) M. H. Whangbo, H. B. Schlegel, and S. Wolfe, *J. Am. Chem. Soc.*, **99**, 1296 (1977).
(10) J. A. J. Jarvis, B. T. Kilbourn, and P. B. Owston, *Acta Crystallogr., Sect. B*, **27**, 876 (1971).
(11) J. G. Norman, Jr., *Inorg. Chem.*, **16**, 1328 (1977).
(12) E. J. Baerends, D. E. Ellis, and P. Ros, *Chem. Phys.*, **2**, 41 (1973).
(13) M. J. S. Dewar, *Bull. Soc. Chim. Fr.*, **18**, C71 (1951).
(14) H. W. Quinn and J. H. Tsai, *Adv. Inorg. Chem. Radiochem.*, **12**, 217 (1969).
(15) P. Brandt, *Acta Chem. Scand.*, **13**, 1639 (1959).
(16) H. Hosoya and S. Nagakura, *Bull. Chem. Soc. Jpn.*, **37**, 249 (1964); S. Sakaki, *Theor. Chim. Acta*, **30**, 159 (1973); R. D. Bach and H. F. Henneike, *J. Am. Chem. Soc.*, **92**, 5589 (1970).
(17) H. Basch, *J. Chem. Phys.*, **56**, 441 (1972).
(18) W. C. Hamilton, K. A. Klanderman, and R. Spratley, *Acta Crystallogr., Sect. A*, **25**, S172 (1969).
(19) L. M. Muir, K. W. Muir, and J. A. Ibers, *Discuss. Faraday Soc.*, **47**, 84 (1969).
(20) S. D. Ittel and J. A. Ibers, *Adv. Organomet. Chem.*, **14**, 33 (1976).
(21) J. Chatt and L. A. Duncanson, *J. Chem. Soc.*, 2939 (1953).
(22) D. M. P. Mingos, *Adv. Organomet. Chem.*, **15**, 1 (1977).
(23) N. Rösch, R. P. Messmer, and K. H. Johnson, *J. Am. Chem. Soc.*, **96**, 3855 (1974).

Contribution from the Gibbs Chemical Laboratory,
Harvard University, Cambridge, Massachusetts 02138

Molecular Orbital Studies of *nido*-Beryllaboranes, $B_5H_{10}BeX$, Where X Is BH_4, B_5H_{10}, CH_3, or C_5H_5

JOZEF BICERANO and WILLIAM N. LIPSCOMB*

Received December 6, 1978

Molecular orbital studies are presented at the minimum basis set level for the beryllaboranes $B_5H_{10}BeBH_4$, $B_5H_{10}BeB_5H_{10}$, $B_5H_{10}BeCH_3$, and $B_5H_{10}BeC_5H_5$. The method, nearly at the SCF level, employs the PRDDO (partial retention of diatomic differential overlap) program. The bonding is analyzed in terms of charge stability, static reactivity indices, degrees of bonding, overlap populations, and fractional bonds obtained from localized molecular orbitals by using the criterion of Boys. The bonding within B_5H_{10} units is remarkably similar, although bonding about Be in $B_5H_{10}BeC_5H_5$ differs significantly from that in the other compounds. The relationships of these studies to the NMR spectra and to related chemistry are briefly indicated.

Introduction

The high toxicity of beryllium compounds[1] has limited studies in a very promising area of chemistry. Nevertheless, in the past decade a number of new beryllaboranes have been